Specialty area: **Imaging Acquisition & Reconstruction**

Speaker name: Michael Garwood, gar@cmrr.umn.edu

Highlights

- Due to the non-linearity of the Bloch equations, the bandwidth of amplitude-modulated (AM) pulses varies with flip angle, and this should be considered in sequence design.
- Frequency-modulated (FM) pulses can provide tolerance to B_1-variation and some require less peak RF power than the equivalent bandwidth-matched AM pulse.
- Powerful methods are available to design and optimize the performance of RF pulses; one of these known as the Shinnar-Le Roux (SLR) algorithm uses a hard pulse approximation, allowing the pulse to be described by two complex polynomials.
- One- and multi-dimensional pulses can be designed using a k-space description in a low-flip-angle approximation.
- Pulse design methods such as VERSE and GOIA use gradient modulation to reduce RF energy deposition (SAR).

Talk title: **RF Pulses Designs: from Basics to the State-of-the-Art**

- **Target audience**: MRI scientists and pulse sequence developers
- **Outcomes/Objects**: Attendees will gain insight into the physics of RF pulses, the different types of RF pulses, and the tools and methods available to design and optimize their performance.
- **Purpose**: This presentation is meant to provide the general framework and formalisms for understanding and designing different types of RF pulses used in MRI sequences.
- **Methods**:

1) *Visualizing the rotations produced by RF pulses:*

A rotating coordinate frame (x'y'z') provides the best platform from which to visualize the motion of a magnetization vector $\mathbf{M}$ experiencing the torque from a magnetic field vector $\mathbf{B}$. In a reference frame rotating about $\mathbf{B_0}$ at the angular velocity ω_{RF} of the RF field, the on-resonance condition occurs when the RF frequency is equal to the Larmor frequency; that is, when $\omega_{RF} = \omega_0$ (Fig. 1a). In the on-resonance case, the signal intensity following a pulse having duration T_p will be proportional to $\sin\theta$, where

$$\theta = \int_0^{T_p} \omega_1(t)\,dt\,.$$

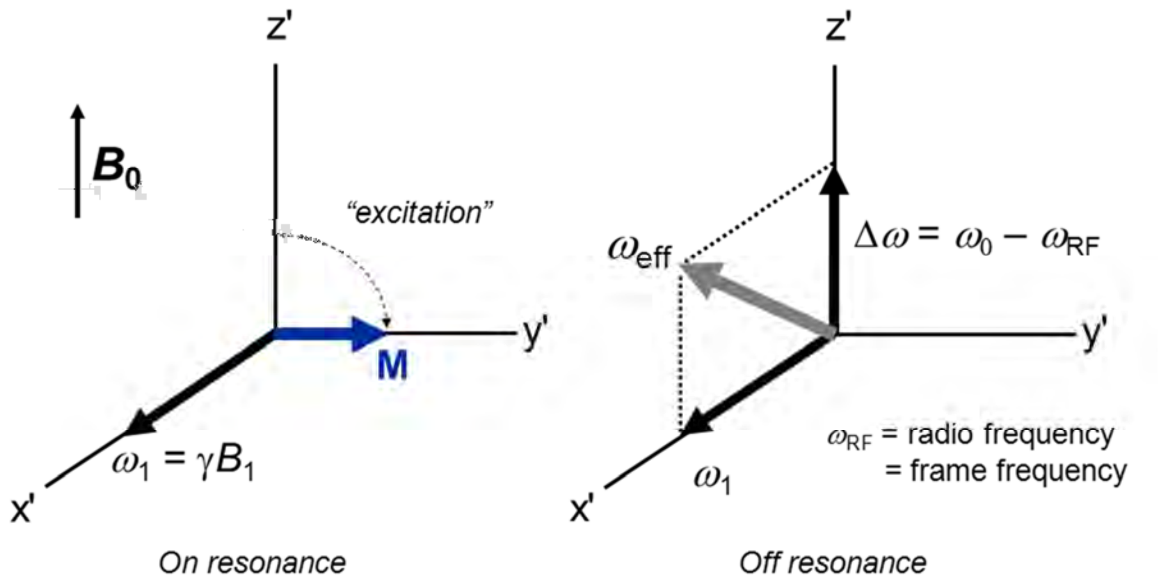

Figure 1: A rotating frame of reference showing the magnetic field components as angular velocity vectors, $\omega_1\hat{\mathbf{i}}$ and $\Delta\omega\hat{\mathbf{k}}$, for the case in which the RF pulse is applied (a) on resonance and (b) off resonance.

An important feature of any RF pulse is how uniformly it rotates **M** despite an offset $\Delta\omega$ that occurs, for example, in the presence of a field gradient used for slice selection. In the off-resonance case, the axis of rotation is tilted out of the transverse plane (Fig. 1b).

2) Types of RF pulses and their features:

The pulse shapes most often used in MRI are amplitude-modulated (AM). Common examples include pulses having shapes defined by sinc and gauss functions. These originated in the early days of MRI and were derived from a Fourier transform (linear) approximation to the Bloch equations. The frequency offset ($\Delta\omega$) range over which a pulse rotates the magnetization is known as the pulse bandwidth, b_w. The bandwidth is inversely proportional to T_p and depends on the specific pulse pattern (e.g., sinc versus gauss) and the flip angle that is used. The latter is a consequence of the non-linearity of the Bloch equations. When developing multi-slice spin-echo and other multi-pulse sequences, T_p of the 90° pulse (or 180° pulse) should be adjusted so that $b_w(90°)= b_w(180°)$. Table 1 gives the factors that can be used to calculate b_w for some common pulse shapes when using θ = 90° and 180°. These were obtained by using Bloch simulations.

With AM pulses, the carrier frequency (ω_{RF}) remains constant during RF irradiation. With another class of pulses known as frequency-modulated (FM) pulses, the pulse is both amplitude- and frequency-modulated. This difference is illustrated in Fig 2. Common FM pulses are the chirp and hyperbolic secant (HS) pulses (1-5). A comparison of the slice profiles produced by sinc and HS pulses is shown in Fig 3. An adiabatic pulse is an FM pulse satisfying certain conditions described below.

Table 1:

Bandwidth factors of different pulse shapes and flip angles determined from Bloch simulations:

b_w = factor/T_p

where b_w is bandwidth in Hertz at full width half maximum (FWHM)

Pulse	***factor***
90° square	1.4
180° square	0.8
90° gauss	2.7
180° gauss	1.5
90° sinc (5 lobe)	5.9
180° sinc (5 lobe)	4.5
hyperbolic secant (AFP)	$\Delta\omega_{max} T_p/\pi$

With an FM pulse, ω_{RF} is time dependent, and therefore, the amplitude of $\Delta\omega\hat{\mathbf{k}}$ and the amplitude and orientation of $\vec{\omega}_{eff}$ change during the pulse. Here we briefly describe the motions of the time-dependent magnetization and the field components in a rotating frame, in response to an FM pulse. At any moment during the pulse, the rate at which $\vec{\omega}_{eff}(t)$ changes its orientation is given by the instantaneous angular velocity, d$\alpha(t)$/dt, where α is the angle between $\vec{\omega}_{eff}$ and the z'-axis. At the beginning of the pulse (t = 0), if $\Delta\omega$ >>0, then the magnitude of $\Delta\omega\hat{\mathbf{k}}$ is very large relative to that of $\omega_1\hat{\mathbf{i}}$, and thus, the initial orientation of $\vec{\omega}_{eff}$ will be approximately collinear with z'. As $\omega_{RF}(t)$ increases during the pulse, $\Delta\omega$ decreases and $\vec{\omega}_{eff}(t)$ rotates toward the transverse plane. When $\omega_{RF}(t)$ = ω_0, the orientation of $\vec{\omega}_{eff}$ is parallel to $\omega_1\hat{\mathbf{i}}$, regardless of the magnitude of the $\omega_1\hat{\mathbf{i}}$. In a classical adiabatic half-passage (AHP), the orientation of $\vec{\omega}_{eff}$ is swept in this manner from z' to an axis in the transverse plane. In an adiabatic full-passage (AFP), the sweep of $\omega_{RF}(t)$ is continued past resonance so that the final orientation of $\vec{\omega}_{eff}$ is parallel with -z' (i.e., at

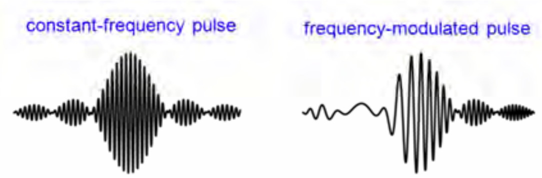

Figure 2: The difference between an AM only pulse (left) and a pulse that is both amplitude and frequency-modulated (right). Note that the frequency of the carrier under the sinc-shaped AM envelope varies in time in the FM case.

the end of the AFP, $\Delta\omega$<<0). During an adiabatic pulse, a magnetization vector (**M**) which is parallel to $\vec{\omega}_{eff}$ will tend to follow $\vec{\omega}_{eff}$, provided that $|\vec{\omega}_{eff}(t)| >> |d\alpha(t)/dt|$, for all t. This inequality is known as the "adiabatic condition". In simple terms, the adiabatic condition states that, at all times during the pulse, the rate at which $\vec{\omega}_{eff}$ changes its orientation must be small relative to the rate at which a magnetization vector rotates about $\vec{\omega}_{eff}$. Adiabatic pulses can be designed to tolerate extreme B_1-inhomogeneity. As shown in Fig. 3, above a threshold RF amplitude the HS pulse operates adiabatically and thus continues to invert magnetization despite a further increase of RF amplitude.

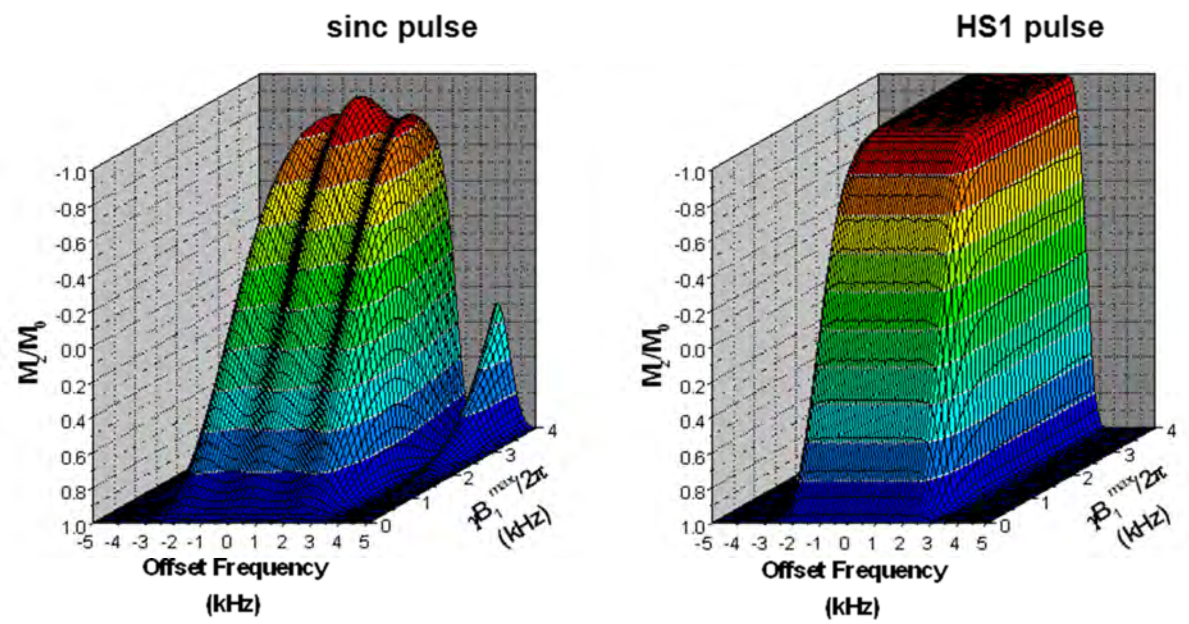

Figure 3: Slice profiles produced by sinc and hyperbolic secant (HS1) pulses as a function of RF amplitude, B_1^{max}. It can be seen that the slice profile of the sinc varies as a function of B_1^{max} and displays undesirable side-lobes at the higher RF amplitudes. On the other hand, the slice produced by the HS1 pulse remains highly invariant as the RF amplitude changes.

A desirable feature of certain FM pulses is their ability to perform a similar rotation of **M** using lower RF amplitude than the equivalent (bandwidth-matched) AM pulse. On the other hand, for given settings of flip angle and b_w, the RF energy deposited by different RF pulses (both AM and FM pulses) is the same. That is, for given flip angle and b_w, SAR remains fixed when using different pulse shapes. On the surface, this may not seem to be true, and a more careful look is required to understand why. Table 2 lists pulse duration, RF amplitude and relative SAR (E_{rel}) of sinc and HS pulses when rotating longitudinal magnetization (M_z) in a slice of b_w = 5 kHz (FWHM). It can be seen that E_{rel} of the 180° HS pulse appears to be 35% larger than that of the sinc pulse, and this therefore appears to contradict the statement above. However, after viewing the slice profiles in Fig. 4, it can be appreciated why the HS appears to deposit more RF energy. That is, the sinc pulse rotates to a flip angle much smaller than the desired value over much of the bandwidth (i.e., away from the slice center, M_z>-0.9M_0), and only in this way is the sinc able to use lower SAR than the HS pulse. Note, Table 2 also shows that the duration of the HS pulse is >4-fold longer than the sinc pulse. FM pulses generally require a longer T_p than the equivalent AM pulse, which in some cases is a disadvantage.

Table 2:

Comparison of Pulses
for M_z bandwidth (FWHM) = 5 kHz

Pulse	T_p (ms)	$\gamma B_1^{max}/2\pi$ (kHz)	E_{rel}^*
90° sinc	1.05	1.44	1.0
90° HS†	4.0	0.71	0.99
180° sinc⁺	0.90	2.68	1.0
180° HS†⁺	4.0	1.42	1.35

* E_{rel} = relative RF energy, $\int_0^{T_p} B_1^2(t)dt$
† Hyperbolic secant pulse created with $\Delta\omega_{max}T_p/\pi$ = 20
⁺ 180° flip angle defined as M_z= -0.9M_0 on resonance

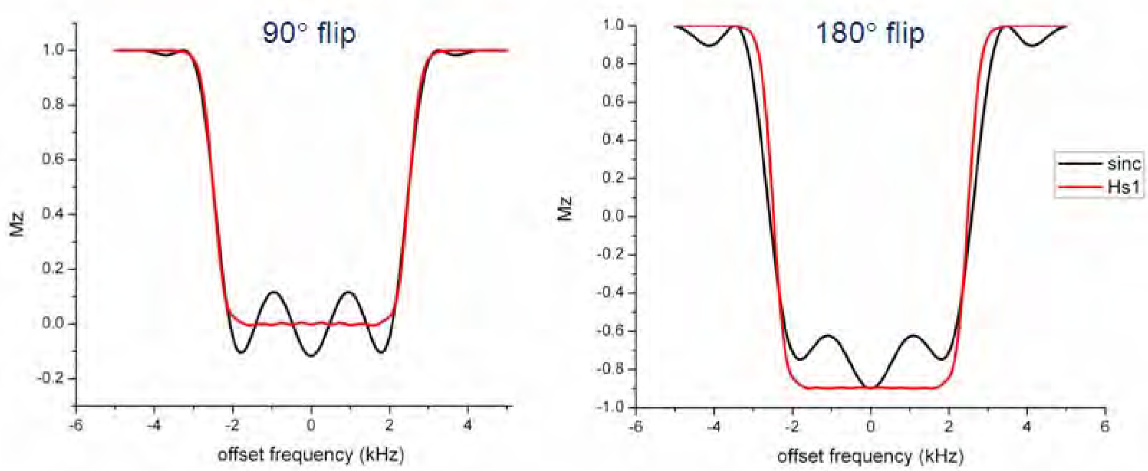

Figure 4: Slice profiles (M_z) of the sinc and HS1 pulse for flip angles = 90º (left) and close to 180º (right).

3) Design and optimization methods:

So far, the only AM pulses discussed were those obtained from a linear approximation (i.e., FT) to the Bloch equations. However, several methods have been developed to obtain solutions to the Bloch equations and these have shown great utility for generating both AM and FM pulses with improved performance specifications (e.g., see Refs (3,6-15)). The Shinnar-Le Roux (SLR) algorithm is probably the most popular method to generate pulses for slice selection (e.g., for excitation pulses that produce a flat baseband with sharp boundaries). A key to the SLR algorithm is the so-called hard-pulse approximation allowing the RF pulse to be mapped into two complex polynomials (called the forward SLR transform). During a pulse, **M** is rotating about the vector sum of $\omega_1\hat{\mathbf{i}}$ and $\Delta\omega\hat{\mathbf{k}}$ due to the gradient field. The basic idea of the hard-pulse approximation is that, if the angle is small, the rotation can be modeled by two sequential rotations. Given the two related polynomials, the inverse SLR transform is used to calculate the RF pulse that produces these polynomials. This inverse transform reduces RF pulse design to polynomial design. The Shinnar-Le Roux algorithm is fast and slice profiles can be calculated analytically.

Another major advance in RF pulse design came with the development of the k-space description of RF pulses that assumes a low flip angle approximation (16). This formalism led to not only new types of one-dimensional slice-selective pulses, but also multi-dimensional RF pulses.

Finally, valuable methods have been developed to reduce the RF energy deposited (SAR) during slice selection using gradient modulation. Two such methods are known as VERSE (17) and GOIA (18).

References

1. Dunand J-J, Delayre J; Impulse response magnetic resonance spectrometer. U.S. patent 3,975,675. 1976.
2. Silver MS, Joseph RI, Chen CN, Sank VJ, Hoult DI. Selective population inversion in NMR. Nature 1984;310(5979):681-683.
3. Silver MS, Joseph RI, Hoult DI. Highly selective $\pi/2$ and π pulse generation. J Magn Reson 1984;59:347-351.
4. Garwood M, DelaBarre L. The return of the frequency sweep: designing adiabatic pulses for contemporary NMR. J Magn Reson 2001;153(2):155-177.
5. Tannús A, Garwood M. Improved performance of frequency-swept pulses using offset-independent adiabaticity. J Magn Reson A 1996;120:133-137.
6. Murdoch JB, Lent AH, Kritzer MR. Computer-optimized narrowband pulses for multislice imaging. Journal of Magnetic Resonance (1969) 1987;74(2):226-263.
7. Ngo JT, Morris PG. General solution to the NMR excitation problem for noninteracting spins. Magnetic Resonance in Medicine 1987;5(3):217-237.
8. Shinnar M, Bolinger L, Leigh JS. The use of finite impulse response filters in pulse design. Magnetic Resonance in Medicine 1989;12(1):81-87.

9. Carlson JW. Exact solutions for selective-excitation pulses. Journal of Magnetic Resonance (1969) 1991;94(2):376-386.
10. Pauly J, Le Roux P, Nishimura D, Macovski A. Parameter relations for the Shinnar-Le Roux selective excitation pulse design algorithm [NMR imaging]. Medical Imaging, IEEE Transactions on 1991;10(1):53-65.
11. Buonocore MH. The analytic theory, optimization, and performance of transparent pulses. Magnetic Resonance in Medicine 1992;24(2):314-324.
12. Rourke DE, Morris PG. The inverse scattering transform and its use in the exact inversion of the bloch equation for noninteracting spins. Journal of Magnetic Resonance (1969) 1992;99(1):118-138.
13. Buonocore MH. RF pulse design using the inverse scattering transform. Magnetic Resonance in Medicine 1993;29(4):470-477.
14. Rourke DE, Bush SD. Inversion of the Bloch equations with T_2 relaxation: An application of the dressing method. Physical Review E 1998;57(6):7216 LP - 7230.
15. Balchandani P, Pauly J, Spielman D. Designing adiabatic radio frequency pulses using the Shinnar–Le Roux algorithm. Magnetic Resonance in Medicine 2010;64(3):843-851.
16. Pauly J, Nishimura D, Macovski A. A k-space analysis of small-tip-angle excitation. J Magn Reson 1989;81:43-56.
17. Conolly S, Nishimura D, Macowski A. Variable-rate selective excitation. J Magn Reson 1988;78:440-458.
18. Tannus A, Garwood M. Adiabatic pulses. NMR Biomed 1997;10(8):423-434.